Applied Catalysis B: Environmental 98 (2010) 132–137

Contents lists available at ScienceDirect

Applied Catalysis B: Environmental

journal homepage: www.elsevier.com/locate/apcatb

Effect of pore morphology of mesoporous carbons on the electrocatalytic activity of Pt nanoparticles for fuel cell reactions

Shuqin Song[a], Yeru Liang[b], Zhenghui Li[b], Yi Wang[a], Ruowen Fu[b], Dingcai Wu[b,**], Panagiotis Tsiakaras[c,*]

[a] State Key Laboratory of Optoelectronic Materials and Technologies, School of Physics and Engineering, Sun Yat-sen University, Guangzhou 510275, China
[b] Materials Science Institute, PCFM Laboratory, School of Chemistry and Chemical Engineering, Sun Yat-sen University, Guangzhou 510275, China
[c] Department of Mechanical Engineering, School of Engineering, University of Thessaly, Pedion Areos 38834, Greece

ARTICLE INFO

Article history:
Received 26 February 2010
Received in revised form 15 May 2010
Accepted 19 May 2010
Available online 26 May 2010

Keywords:
Pore morphology
Mesoporous carbon
Pt nanoparticles
PEM fuel cells
Ethanol electrooxidation
Oxygen reduction reaction

ABSTRACT

In the present investigation, the role of the pore morphology of mesoporous carbons in the electrocatalytic activity of Pt nanoparticles for fuel cell reactions has been successfully revealed by adopting ordered mesoporous carbon CMK-3 and disordered wormhole-like mesoporous carbon (WMC) as the support material, respectively. Both materials possess very similar pore characteristics (pore volume, BET surface area, mesopore size) except pore morphology. It has been found that CMK-3 can provide Pt nanoparticles with more electrochemically active Pt sites and higher electrochemical surface area, and thus, Pt/CMK-3 exhibits superior fuel cell reactions activity compared to Pt/WMC, especially in the case of liquid reactants (e.g. ethanol). This could be attributed to the much easier mass transportation through CMK-3 support profiting from both the high ordered degree and the very good 3D interconnection of the nano-spacings of their hexagonally arrayed carbon nanorods (i.e. mesopores), thus leading to more accessibility of Pt nanoparticles. The above results demonstrates that the pore morphology of carbon supports plays a decisive role in the electrocatalytic activity of their supported Pt nanoparticles, although other structure parameters like pore size are very similar.

1. Introduction

Proton exchange membrane fuel cells (PEMFC) are expected to be promising clean energy conversion systems in the area of portable power and transportation due to their advantages of low operating temperature and fast start-up [1–3]. For the desirable activity and stability of PEMFC, platinum is generally adopted as the catalyst for oxygen reduction and fuel oxidation, which is the major cost factor resulting in the high cost of fuel cells [4]. To address this, one of the effective measurements is to disperse the Pt nanoparticles onto the non-precious support. Among them, carbon materials have been extensively applied for its excellent virtues of high electrical conductivity, chemical stability in both acidic and basic media, easy modification of surface chemistry, and low cost [5,6].

Up to now, many different carbon nanomaterials, such as activated carbon [7–9], carbon black [10–12], carbon nanotubes (CNTs) [13–16], carbon nanofibers [17,18], mesoporous carbon [19–27], have been attempted. Most of the researches are focused on the effect of the surface area, pore size, and surface chemistry of carbon supports on catalysts activity and stability. Takasu et al. [12], for example, have observed significant effect of the specific surface area of carbon black support on the fundamental properties of PtRu/C, including metal particle size, alloying extent, and their corresponding catalytic activity for methanol electrooxidation. Our previous work [25] demonstrated that the pore size effect of carbon nanomaterials was surprisingly decisive for the accessibility of Pt nanoparticles and consequently their utilization efficiency and electrocatalytic activity. At the same time, it is recognized that the carbon surface chemistry plays an important role in the synthesis of optimised catalysts, and this consequently affects the catalysts performance. Carbon nanotubes were functionalized with many oxygen-containing groups and high graphitisation degree, which provided Pt/CNTs with high electrochemical surface area, high Pt utilization efficiency, and superior activity for the reaction of oxygen reduction [16].

Based on the literature, it can be inferred that the surface area, pore size, and surface chemistry are the very important properties of carbon nanomaterials in terms of catalysts performance and consequently their end-use application. However, to the best of our knowledge, few concerns about the pore morphology effect of carbon nanomaterials on the behaviour of catalysts, most likely due

* Corresponding author. Tel.: +30 24210 74065; fax: +30 24210 74050.
** Corresponding author. Tel.: +86 20 84112759; fax: +86 20 84115112.
E-mail addresses: wudc@mail.sysu.edu.cn (D. Wu), tsiak@mie.uth.gr (P. Tsiakaras).

0926-3373/$ – see front matter © 2010 Elsevier B.V. All rights reserved.
doi:10.1016/j.apcatb.2010.05.021

to lack of appropriate carbon support models as the investigated objects.

Herein, two kinds of mesoporous carbon materials as Pt nanoparticles support are adopted. One is CMK-3 with highly ordered structure, in which the hexagonally arrayed carbon nanorods are interconnected by spacers, which are constituted by the carbon that filled the channel-interconnecting micropores in the pore wall of SBA-15 template [24]. The other is wormhole-like mesoporous carbon (WMC), which is of a disordered three-dimensional nano-network structure [26]. Both have similar pore parameters (pore volume, BET surface area, mesopore size), and they are obtained from the same carbon source (sucrose) with the same carbonization technique, thus possessing the same surface chemistry. With them as the support materials for Pt nanoparticles, the obtained catalysts were adopted for both ethanol electrooxidation and oxygen reduction reaction. Although so, it has been surprisingly found that the different pore morphology has a significant effect on the electrocatalytic activity of Pt for fuel cell reactions.

2. Experimental

2.1. Preparation of carbon nanomaterials

According to the procedure in the literatures [24,26], the synthesis of CMK-3 and WMC was carried out using SBA-15 and silica gel as the template, respectively. Both carbon samples were from sucrose and underwent the same carbonization process (3 h at 900 °C with a heating rate of 5 °C min^{-1} in N_2 flow). The typical preparation procedure was described as follows.

In the case of WMC: a quantity of sucrose was dissolved in 3 mL of H_2SO_4 aqueous solution followed by adding tetraethylorthosilicate (TEOS) (sucrose:H_2SO_4 solution:TEOS = 2 g:3 mL:4 mL). The mixture was stirred continuously until complete homogenization. Subsequently, 4 wt% hydrofluoric acid (HF) solution (HF/TEOS molar ratio = 1/30) was added under stirring. The obtained homogeneous mixture was quickly gelated and aged in an open plastic bottle at 40 °C for 2 days. The resulting composites were further reacted for 6 h at 100 °C and subsequently for 6 h at 160 °C. Then the sample was heated to 900 °C at a heating rate of 5 °C min^{-1}, and kept at this carbonization temperature for 3 h in N_2 flow. After that, the carbon/silica composites were washed using HF solution to obtain WMC.

In the case of CMK-3: SBA-15 was added to a solution obtained by dissolving sucrose and H_2SO_4 in H_2O. The mixture was reacted for 6 h at 100 °C and subsequently for 6 h at 160 °C. After the same treatment procedure as that of WMC as described above, the carbon/SBA-15 composites were washed using HF solution to obtain CMK-3.

2.2. Preparation of electrocatalysts

Pt/CMK-3 and Pt/WMC catalysts with the Pt loading of 20 wt% were obtained by a pulse-microwave assisted polyol synthesis procedure as described in our previous work [28,29]. Typically, an appropriate amount of $H_2PtCl_6{\cdot}6H_2O$ was well mixed with ethylene glycol (EG) in an ultrasonic bath, and then the as-prepared carbon nanomaterials as the support was added into the mixture. After the pH value of the system was adjusted to more than 10 by the dropwise addition of 1.0 mol L^{-1} NaOH/EG, the well-dispersed slurry was obtained with stirring and ultrasonication for 30 min. Thereafter, the slurry was microwave-heated in the on/off pulse form at 5 s/5 s for several times and then re-acidified. Finally, the resulting black solid sample was filtered, washed with hot water until no chloride anion in the filtrate could be detected by 1.0 mol L^{-1} $AgNO_3$ aqueous solution and then dried at 80 °C for 10 h in a vacuum oven.

2.3. Characterization of catalysts

The low-angle X-ray diffraction (XRD) patterns were recorded on a D-MAX 2200 VPC diffractometer using Cu Kα radiation (40 kV, 30 mA). N_2 adsorption-desorption measurements were carried out using a Micromeritics ASAP 2010 analyzer at 77 K. The BET surface area (S_{BET}) and the mesopore volume (V_{mes}) were determined by BET theory and BJH method, respectively. The wide-angle XRD measurements were carried out by the aid of a D/Max-IIIA (Rigaku Co., Japan) employing Cu Kα (λ = 0.15406 nm) as the radiation source at 40 kV and 40 mA. The transmission electron microscopy (TEM) investigations were carried out in a JEOL TEM-2010(HR) operating at 200 kV to get information of the mean particle size and size distribution of Pt particles of the catalysts. The histogram of the as-prepared Pt-based catalysts was made by measuring more than 300 particles. For sample preparation, the catalysts were ultrasonically dispersed in ethanol solution to get uniform catalyst ink and fixed onto a copper grid covered with holey carbon film.

All the electrochemical measurements were conducted on a PARSTAT 2273 instrument in a three-electrode cell mounted in a thermostatic water bath, with a saturated calomel electrode (SCE) as the reference electrode and a platinum foil as the counter electrode, respectively. The catalyst thin film was prepared onto the glassy carbon disk surface with a diameter of 0.5 cm. Typically, a mixture containing 5.0 mg electrocatalyst, 1.80 mL ethanol and 0.20 mL Nafion solution (5 wt%, density: 0.874 g mL^{-1} at 25 °C, DuPont, USA) was ultrasonicated for 15 min to obtain a well-dispersed ink. The catalyst ink was then quantitatively transferred onto the surface of the glassy carbon electrode and dried under infrared lamp to obtain a catalyst thin film. The Pt loading was maintained to be 25.5 μg Pt cm^{-2}. The electrochemical tests were performed: (i) in 0.5 mol L^{-1} H_2SO_4 aqueous solution for the characterization of the electrochemical surface area (ESA), and (ii) in 0.5 mol L^{-1} H_2SO_4 aqueous solution containing 1.0 mol L^{-1} C_2H_5OH for the evaluation of the electrocatalytic activity. Before each experiment, the electrolyte solution was bubbled with high-purity N_2 for 30 min to remove the dissolved oxygen inside. In order to also investigate their activity towards oxygen reduction reaction (ORR), rotating disk electrode (RDE) tests were carried out in an O_2-saturated 0.5 mol L^{-1} H_2SO_4 solution with a potential range from 1.1 to 0.1 V at a rotating speed of 1600 rpm and a scan rate of 10 mV s^{-1}. Before each measurement, the working electrodes were electrochemically cleaned by continuous cycling at 50 mV s^{-1} until a stable response was obtained. For the cyclic voltammetry (CV) measurements, after the electrode cleaning, the potential scanning cycles were set to be 15 and the 15th cycle data was used for comparison. It should be noted that the potential is referred to the reversible hydrogen electrode (RHE) without specification.

3. Results and discussion

3.1. Physico-chemical characterization

Fig. 1(A) depicts the low-angle XRD patterns of the as-prepared CMK-3 and WMC samples. It can be seen that CMK-3 possesses an intense diffraction peak (1 0 0) and two resolved diffraction peaks (1 1 0) and (2 0 0), indicating high periodic order arrangement of symmetry mesopores in CMK-3 [24]. For such a material, these mesopores are parallel and straight [24]. Comparatively, no diffraction peaks in the XRD patterns are observed for WMC, indicative of thoroughly disordered mesopore arrangement. The sinuate wormhole-like mesopores extend throughout the structure of WMC [26]. The pore structure of CMK-3 and WMC samples are further investigated by N_2 adsorption–desorption isotherms as

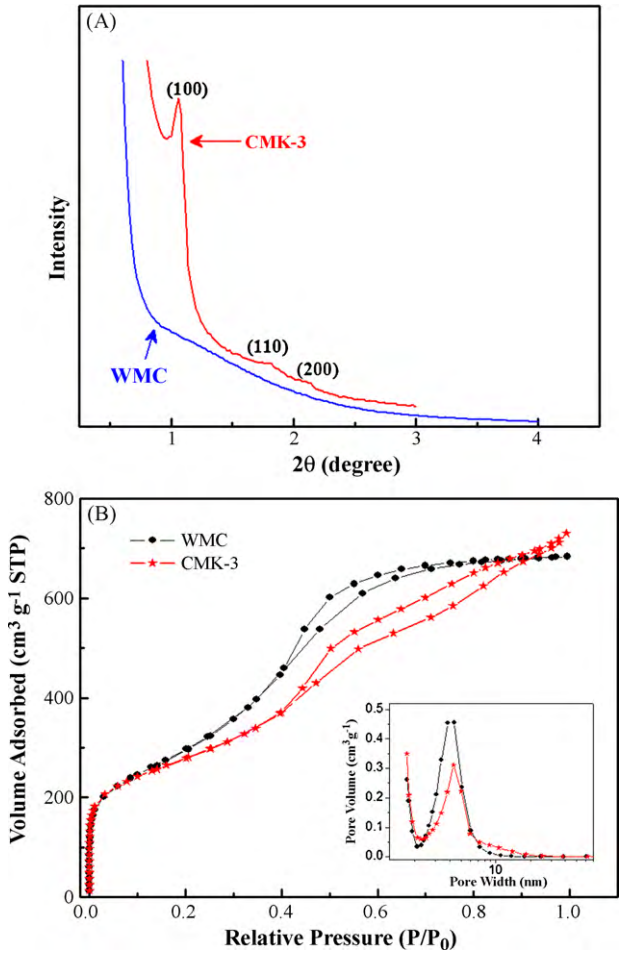

Fig. 1. (A) Low-angle XRD patterns of CMK-3 and WMC samples and (B) N_2 adsorption–desorption isotherms of CMK-3 and WMC samples (the inset shows their BJH pore size distributions).

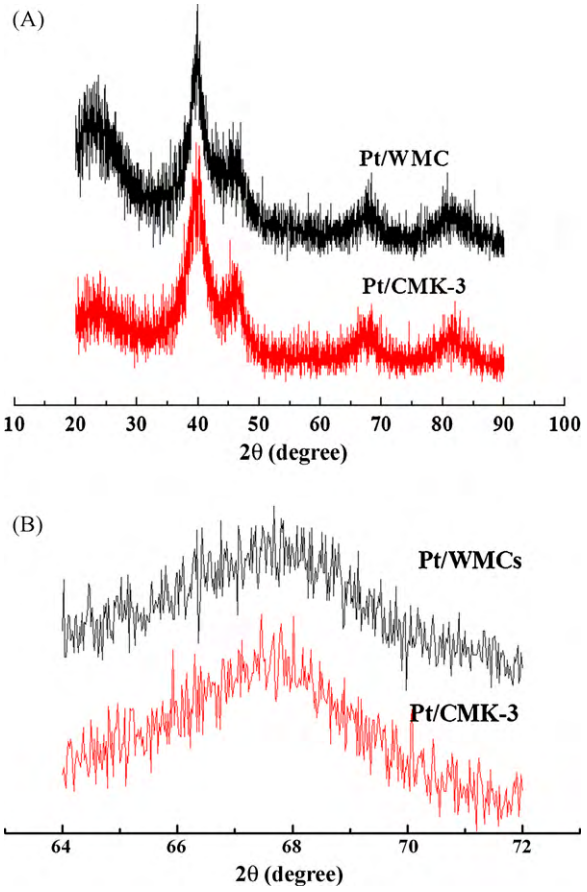

Fig. 2. (A) Wide-angle XRD patterns of Pt/CMK-3 and Pt/WMC and (B) their corresponding (2 2 0) facet.

shown in Fig. 1(B). Both samples exhibit typical type IV isotherms with a distinct hysteretic loop, clearly indicating the mesoporous nature of the as-prepared samples. Moreover, it can be clearly seen from the inset in Fig. 1(B) that both CMK-3 and WMC have a unimodal, narrow pore size distribution with a maximum around 4.3 and 4.4 nm, respectively. The mesopore diameter of CMK-3 is almost the same as that of WMC. Moreover, the BET surface area of WMC is measured to be 1076 $m^2\,g^{-1}$, which is close to the corresponding value of CMK-3 (992 $m^2\,g^{-1}$), and the mesopore volumes are basically identical for these two types of carbons (1.24 and 1.21 $cm^3\,g^{-1}$ for WMC and CMK-3, respectively). The above characterization results clearly demonstrate that the as-prepared WMC and CMK-3 have very similar mesopore structure parameters except for mesopore morphology.

Fig. 2(A) shows the wide-angle XRD results of Pt/WMC and Pt/CMK-3. It can be clearly seen that both samples exhibit the typical characteristics of a crystalline Pt face centered cubic (fcc) structure. The fitted (2 2 0) plane (Fig. 2(B)) was used to calculate the average Pt nanoparticles size according to Scherrer formula [30], with an average particle size of 3.1 nm in both cases, which is further verified by their corresponding TEM images as displayed in Fig. 3. Moreover, it can be seen from Fig. 3 that the Pt nanoparticles are uniformly dispersed on the pore surface of both supports, CMK-3 and WMC. Based on the measurements of 300 particles in random regions, the respective average particle size was estimated to be 3.1 nm for Pt/WMC and 3.2 nm for Pt/CMK-3, which is close to the XRD results.

3.2. Electrochemical surface area

The technique of CV was used to determine the Pt electrochemical surface area of the Pt/WMC and Pt/CMK-3 electrodes. As it can be clearly seen from the CV curves reported in Fig. 4, Pt/CMK-3 shows stronger peaks characteristics of hydrogen desorption in the potential range between 0 and 0.35 V than Pt/WMC. This demonstrates that Pt/CMK-3 has a higher electrochemical surface area. For detailed information, integrating the charge in this range, it is possible to calculate the electrochemical surface area (S_{ESA}) of Pt by using Eq. (1):

$$S_{ESA}\ [m^2\ Pt/mg\,Pt] = \frac{\text{charge}\ [\mu C\,cm^{-2}]}{\{210\ [\mu C\,cm^{-2}\,Pt] \times Pt\ \text{loading}\ [mg\,cm^{-2}]\} \times 10^4} \quad (1)$$

According to this equation, the S_{ESA} value of Pt was 39.0 $m^2\,g^{-1}$ and 3.2 $m^2\,g^{-1}$ for Pt/CMK-3 and Pt/WMC, respectively. This indicates that Pt is at least 10 times more electrochemically active (utilized) in the case of Pt/CMK-3 than that of Pt/WMC electrode. These results hint the significant effect of structural morphology of support materials on the accessibility of Pt nanoparticles and consequently their electrochemical activity. Here, it should be noted that compared to the Pt catalyst with Vulcan XC-72 carbon black as the support [31,32], the ESA of Pt/CMK-3 and Pt/WMC is quite low. This could be due to the small pore diameter (*ca.* 4 nm) of both CMK-3 and WMC, which could lead to the blockage of Pt particles inside the pores or encapsulation of Pt particles in the carbon structure. On the other hand, the present results can give an interesting indicator that the pore morphology alone can also significantly affect the

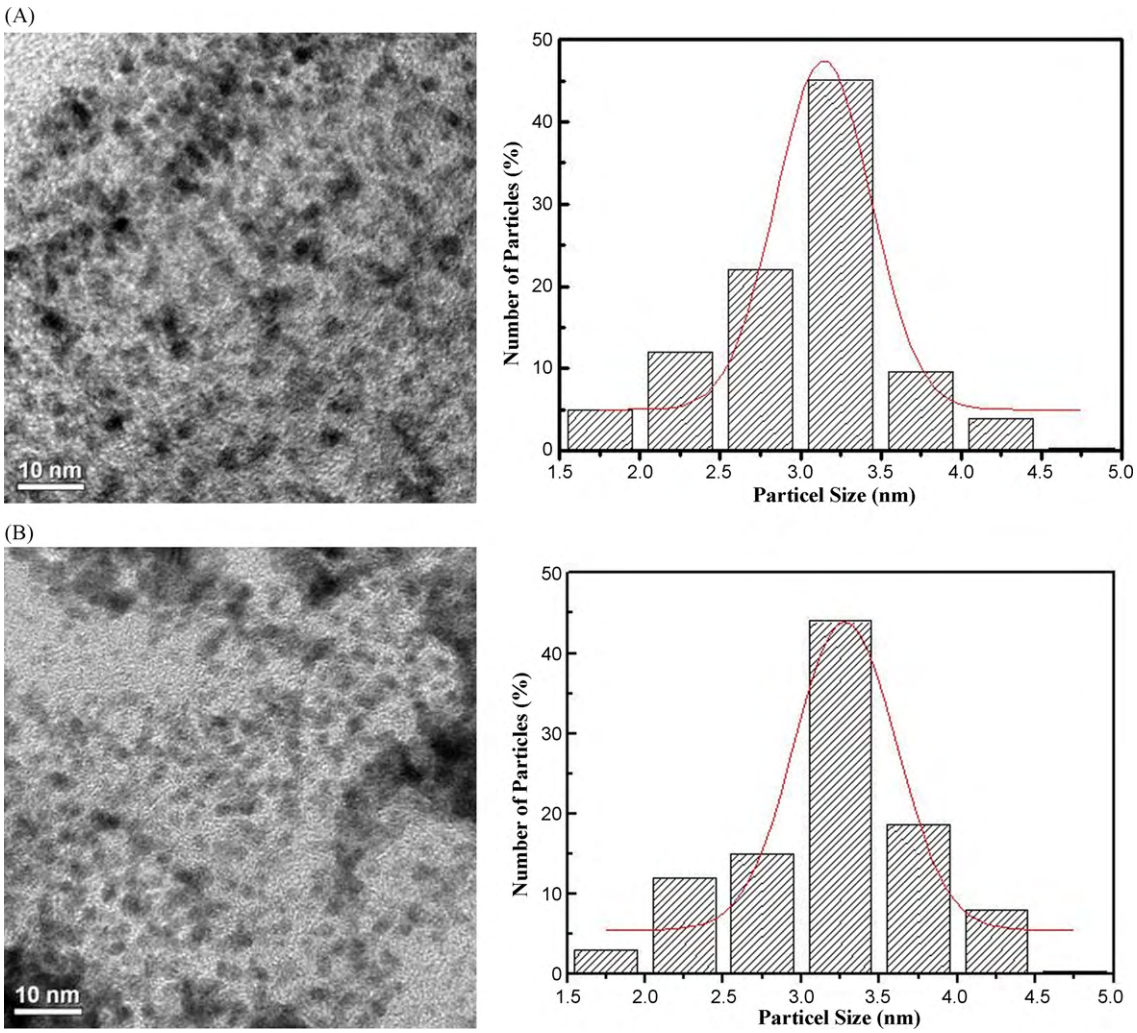

Fig. 3. TEM images of the as-prepared Pt/WMC and Pt/CMK-3 catalysts.

electrocatalytic activity of Pt. It is desirable to develop the mesoporous carbon materials with highly ordered structure and bigger pore diameter (such as about 10 nm) for further investigation.

3.3. Ethanol electrooxidation reaction

In order to evaluate the effect of structural morphology of the carbon support materials on the electrochemical activity of Pt, the Pt/WMC and Pt/CMK-3 catalysts/electrodes were characterized towards the reaction of ethanol electro-oxidation by the aid of the technique of CV adopting a solution of 1.0 mol L^{-1} C_2H_5OH + 0.5 mol L^{-1} H_2SO_4. By comparing the results obtained from the two cases, as shown in Fig. 5(A), it can be distinguished that the obtained CV curves exhibit very prominent characteristic peaks for ethanol electrooxidation. Obviously, Pt/CMK-3 has significantly higher electrocatalytic peak current density than Pt/WMC. More precisely, the specific mass activity of Pt/CMK-3 for ethanol electrooxidation is 758 A/g Pt, which is almost six times higher than that of Pt/WMC. This is an attracting and valuable enhancement for Pt catalysts since the highly ordered carbon as the support materials could significantly reduce both the Pt loading to achieve the same performance and the cost. It is known that a porous electrode has high internal surface area for high electrochemical rates per apparent unit of electrode surface area. However, its internal area cannot, in general, be completely utilized at high current densities due to both mass transfer limitations and ohmic polarization phenomena in the internal pores, simply dependent on the pore structure [25,33]. Based on this, the higher peak current for ethanol electrooxidation, produced in the case of Pt/CMK-3, suggests that the carbon support materials with both the high ordered degree and the very good 3D interconnection of the nano-spacings of their

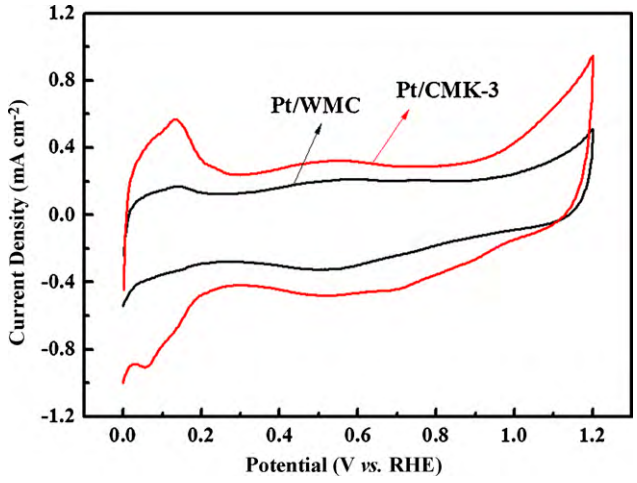

Fig. 4. Cyclic voltammetry curves of the as-prepared Pt/WMC and Pt/CMK-3 catalysts in 0.5 mol L^{-1} H_2SO_4 – scan rate: 20 mV s^{-1}.

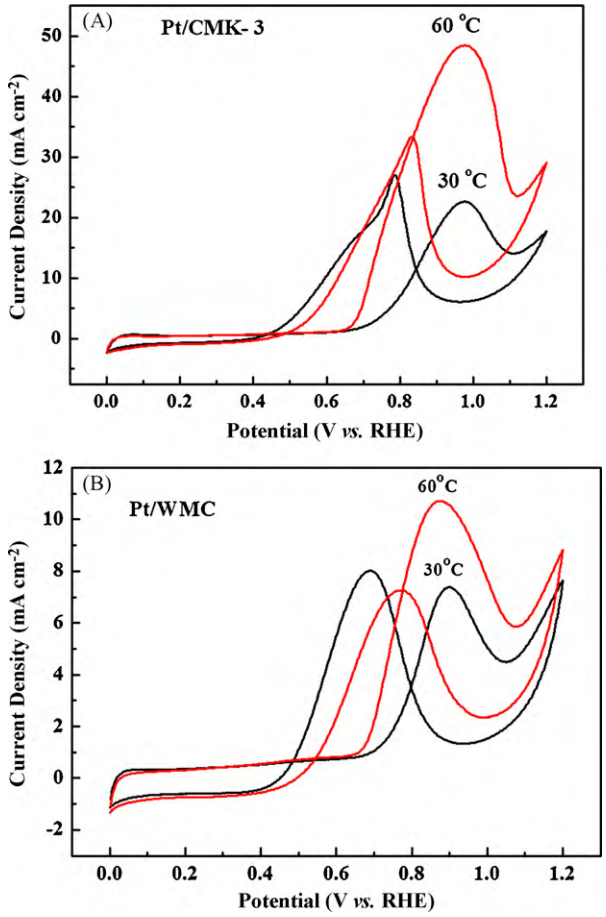

Fig. 5. Cyclic voltammograms of ethanol electro-oxidation on Pt/WMC and Pt/CMK-3 in 0.5 mol L^{-1} H_2SO_4 and 1.0 mol L^{-1} C_2H_5OH solution at different temperatures – scan rate: 50 mV s^{-1}.

hexagonally arrayed carbon nanorods make catalysts possess much higher Pt utilization efficiency than those with disordered structure and sinuate wormhole-like mesopores. This has been proved by the above results as given in Fig. 4.

As known, the reaction rate increases exponentially with temperature. In this way, the mass transport becomes an important factor for higher activity. As displayed in Fig. 5(B), the ethanol electrooxidation activity is enhanced as the temperature increases in both cases. On the other hand, in Pt/CMK-3 case, when the temperature changes from 30 °C to 60 °C, the anodic peak current density increases from 22.6 mA cm^{-2} to 48.43 mA cm^{-2}, with an increment factor of more than 2. While, in Pt/WMC case, the corresponding current density is increased by 1.5 times. At the same temperature, the higher current density in Pt/CMK-3 case indicates that the fine structure regularity and desirable pore morphology of CMK-3 make catalysts possess more available Pt active sites to participate in the electrochemical reaction. The relatively higher incremental factor of anodic peak current density with temperature increment verifies that the highly ordered pores and the very good 3D interconnection in CMK-3 could provide Pt/CMK-3 with easier mass transport and consequently superior performance, which suggests that the carbon materials with ordered structure are suitable and attractive for the use as catalyst support materials in fuel cells.

3.4. Oxygen reduction reaction

For the further evaluation of the effect of structural morphology of support materials on the electrocatalytic activity of Pt, the polarization curves for ORR over Pt/WMC and Pt/CMK-3 were recorded in O_2-saturated 0.5 mol L^{-1} H_2SO_4 employing RDE, and the results are given in Fig. 6. Clearly, Pt/CMK-3 exhibits superior ORR activity to Pt/WMC. Considering from the half wave potential ($E_{1/2}$, the corresponding potential at half of the limiting current density) point of view, it can be found that the respective $E_{1/2}$ value of Pt/CMK-3 and Pt/WMC are 0.657 and 0.614 V. These data clearly show that the half-wave potential in the case of Pt/CMK-3 is positively shifted by 43 mV with reference to that obtained with Pt/WMC as catalyst. This behaviour indicates that Pt/CMK-3 is more active than Pt/WMC towards ORR. As far as the mass activity is concerned, it is known that the mass activity for Pt/C catalysts is the corresponding net kinetic current (i_{kin}) of ORR at a given potential divided by the mass of Pt. The i_{kin} was obtained by using Eq. (2):

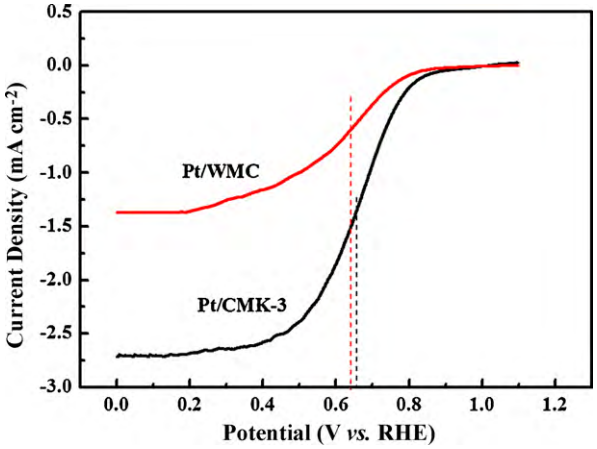

Fig. 6. Polarization curves of the as-prepared Pt/WMC and Pt/CMK-3 catalysts in O_2-saturated 0.5 mol L^{-1} H_2SO_4 at 1600 rpm recorded at a scant rate of 10 mV s^{-1}. The Pt loading was 25.5 μg cm^{-2}.

$$I_{kin} = \frac{i_{lim} \times i_{obs}}{i_{lim} - i_{obs}} \quad (2)$$

where i_{lim} is the limiting current and i_{obs} is the observed current value. Based on the experimental results as shown in Fig. 6 and Eq. (2), it can be found that in the case of Pt/CMK-3 the mass activity corresponds to 229.9 A/g Pt, which is 3.6 times than that of Pt/WMC (63.2 A/g Pt). Such a high activity indicates that several times higher current can be obtained using the same amount of Pt in the case of carbon support materials with fine structural morphology. This will be valuable and practical for reducing the Pt loading in fuel cell catalysts, thus decreasing the fuel cell cost and accelerating its wide use. Furthermore, from Fig. 6 it can also be clearly seen that the ORR current over Pt/CMK-3 begins to rise much more sharply from the onset potential, which can directly improve the cell efficiency. The improved performance could be contributed to highly ordered structure and the very good 3D interconnection of CMK-3 as discussed above, thus facilitating the mass transportation, increasing the electrochemically utilized Pt numbers and enhancing the ORR activity [27].

3.5. The effect of pore morphology

The effect of pore morphology of carbon support materials on the activity of Pt towards fuel cell reactions can be schematically illustrated in Fig. 7. As shown, in the case of Pt/CMK-3, the carbon support CMK-3 has the high ordered degree and the very good 3D interconnection of the nanospacings of their hexagonally arrayed carbon nanorods, resulting in very good mass transportation, and thus, Pt particles can be more easily accessed by the electrolyte. However, in the case of Pt/WMC, both the sinuate pore shape

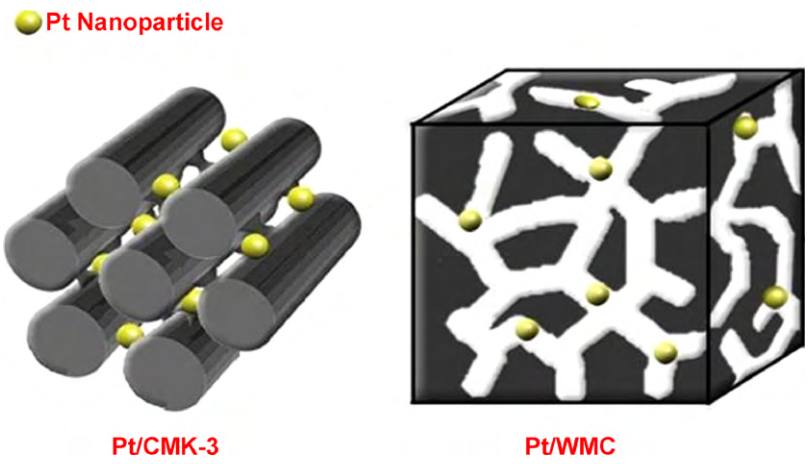

Fig. 7. Schematic illustration for the effect of the pore morphology of carbon support on the activity of Pt nanoparticles.

and relatively low connectivity of the wormhole-like mesopores of WMC are disadvantageous to mass transportation, and thus, many Pt nanoparticles, especially those locating far away from the entrance of the wormhole-like mesopores, will be very hard to be utilized due to poor accessibility. As a result, compared to Pt/WMC, Pt/CMK-3 has a higher electrochemical activity as shown in Figs. 4–6. This suggests that the pore morphology of the carbon support materials indeed plays a decisive role in the catalyst activity.

4. Conclusions

This study clearly presents the effect of pore morphology of mesoporous carbon materials on the electrocatalytic activity of Pt nanoparticles by adopting two different mesoporous carbon (CMK-3 and WMC) as carbon support model. They have the same surface chemistry due to the same carbon source and carbonization process, and have very similar pore structure parameters like pore size (4.3 nm for CMK-3 versus 4.4 nm for WMC) except for the thoroughly different pore morphology. Based on the experimental results, it can be known that the highly ordered structure and the very good 3D interconnection of the nanospacings of their hexagonally arrayed carbon nanorods of CMK-3 can provide Pt nanoparticles with more electrochemically active Pt sites and higher electrochemical surface area. Consequently, Pt/CMK-3 exhibits superior both ethanol electrooxidation and oxygen reduction reaction activity, with the mass activity increased by a factor of 6 and 3.6 times, respectively. From this, one can easily infer that the role of the easier mass transportation benefiting from the desirable pore morphology of mesoporous carbon becomes prominent in the case of liquid reaction (ethanol electro-oxidation). The present work gives an indicator that in the design of the porous materials, the pore morphology should also be considered as a decisive factor for their performance except the pore structural parameters and surface chemistry.

Acknowledgements

This work has been supported by the grant from Hi-Tech Research and Development Program of China (2009AA05Z110), the Project of NSFC (50632040, 50802116, 20903122, and 50972167), the Specialized Research Fund for the Doctoral Program of Higher Education (Nos. 20070558062 and 200805581014), and the Natural Scientific Foundation of Guangdong Province (8451027501001421), and the Project of NSFC (20903122), and the Fundamental Research Funds for the Central Universities (09lgpy30 and 09lgpy18).

References

[1] J. Larminie, A. Dicks, Fuel Cell Systems Explained, second edition, Wiley, 2003.
[2] Z. Qi, Fuel Cells-Proton Exchange Membrane Fuel Cell Systems, Encyclopedia of Electrochemical Power Sources, 2009, pp. 890–900.
[3] S. Song, P. Tsiakaras, Appl. Catal. B: Environ. 63 (2006) 187–193.
[4] X. Yu, S. Ye, J. Power Sources 172 (2007) 133–144.
[5] F. Rodríguez-reinoso, Carbon 36 (1998) 159–175.
[6] A.L. Dicks, J. Power Sources 156 (2006) 128–141.
[7] J. Maruyama, I. Abe, Electrochim. Acta 48 (2003) 1443–1450.
[8] J. Maruyama, K. Sumino, M. Kawaguchi, I. Abe, Carbon 42 (2004) 3115–3121.
[9] M. Kang, Y.-S. Bae, C.-H. Lee, Carbon 43 (2005) 1512–1516.
[10] M. Kim, J.-N. Park, H. Kim, S. Song, W.-H. Lee, J. Power Sources 163 (2006) 93–97.
[11] J.L. Gómez de la Fuente, S. Rojas, M.V. Martínez-Huerta, P. Terreros, M.A. Peña, J.L.G. Fierro, Carbon 44 (2006) 1919–1929.
[12] Y. Takasu, T. Kawaguchi, W. Sugimoto, Y. Murakami, Electrochim. Acta 48 (2003) 3861–3868.
[13] W.Z. Li, C.H. Liang, W.J. Zhou, J.S. Qiu, H.Q. Li, G.Q. Sun, Q. Xin, Carbon 42 (2004) 436–439.
[14] W.Z. Li, C.H. Liang, J.S. Qiu, W.J. Zhou, H.M. Han, Z.B. Wei, G.Q. Sun, Q. Xin, Carbon 40 (2002) 791–794.
[15] K. Shimizu, I.F. Cheng, C.M. Wai, Electrochem. Commun. 11 (2009) 691–694.
[16] S. Yin, P.K. Shen, S. Song, S.P. Jiang, Electrochim. Acta 54 (2009) 6954–6958.
[17] C.D. Taboada, J. Batista, A. Pintar, J. Levec, Appl. Catal. B: Environ. 89 (2009) 375–382.
[18] J.-S. Zheng, X.-S. Zhang, P. Li, X.-G. Zhou, W.-K. Yuan, Catal. Today 131 (2008) 270–277.
[19] H. Yamada, T. Hirai, I. Moriguchi, T. Kudo, J. Power Sources 164 (2007) 538–543.
[20] J. Ding, K.-Y. Chan, J. Ren, F.-S. Xiao, Electrochim. Acta 50 (2005) 3131–3141.
[21] J.S. Yu, S. Kang, S.B. Yoon, G. Chai, J. Am. Chem. Soc. 124 (2002) 9382–9383.
[22] G.S. Chai, S.B. Yoon, J.-H. Kim, J.-S. Yu, Chem. Commun. 11 (2004) 2766–2767.
[23] G.S. Chai, S.B. Yoon, J.-S. Yu, J.-H. Choi, Y.-E. Sung, J. Phys. Chem. B 108 (2004) 7074–7079.
[24] S. Jun, S.H. Joo, R. Ryoo, M. Kruk, M. Jaroniec, Z. Liu, T. Ohsuna, O. Terasaki, J. Am. Chem. Soc. 122 (2000) 10712–10713.
[25] S. Song, S. Yin, Z. Li, P.K. Shen, R. Fu, D. i Wu, J. Power Sources 195 (2010) 1946–1949.
[26] D. Wu, Z. Li, Y. Liang, X. Yang, X. Zeng, R. Fu, Carbon 47 (2009) 916–918.
[27] S.H. Joo, S.J. Choi, I.I. Oh, J. Kwak, Z. Liu, O. Terasaki, R. Ryoo, Nature 412 (2001) 169–172.
[28] S. Song, Y. Wang, P.K. Shen, J. Power Sources 170 (2007) 46–49.
[29] Y. Wang, S. Song, V. Maragou, P.K. Shen, P. Tsiakaras, Appl. Catal. B: Environ. 89 (2009) 223–228.
[30] V. Radmilovic, H.A. Gasteiger, P.N. Ross, J. Catal. 154 (1995) 98–106.
[31] T.J. Schmidt, H.A. Gasteiger, G.D. Stäb, P.M. Urban, D.M. Kolb, R.J. Behm, J. Electrochem. Soc. 145 (1998) 2354.
[32] U.A. Paulus, T.J. Schmidt, H.A. Gasteiger, R.J. Behm, J. Electroanal. Chem. 495 (2001) 134–145.
[33] Y. Qiao, C.M. Li, S.J. Bao, Z.S. Lu, Y.H. Hong, Chem. Commun. 11 (2008) 1290–1292.